Pergamon

Int. J. Heat Mass Transfer. Vol. 37, No. 15, pp. 2193–2201, 1994

0017–9310/94 $7.00 + 0.00

0017–9310(93)E0035–F

A numerical solution for natural convection in an inclined porous cavity with a discrete heat source on one wall

SHIH-WEN HSIAO
Department of Industrial Design, National Cheng-Kung University, Tainan, Taiwan 70101, R.O.C.

CHA'O-KUANG CHEN
Department of Mechanical Engineering, National Cheng-Kung University, Tainan, Taiwan 70101, R.O.C.

and

P. CHENG
Department of Mechanical Engineering, University of Hawaii, Honolulu, HI 96822, U.S.A.

(*Received* 29 *June* 1993 *and in final form* 3 *March* 1994)

Abstract—The problem of steady natural convection in an inclined porous cavity with a discrete heat source on a wall is studied numerically. Non-Darcy and thermal dispersion effects are taken into consideration in the momentum and energy equations, respectively. Wall effects on porosity, permeability and thermal dispersion are also taken into account. The governing equations in terms of vorticity, stream function and temperature are solved numerically by a finite difference method. It is found that a secondary vortex begins to appear in the cavity at a location above the discrete heat source if the media Rayleigh number is sufficiently high; the intensity of the vortex increases with the eccentricity of the heat source and the inclination angle of the cavity. For a porous cavity at zero inclination angle with a vertical wall at a uniform temperature, the predicted average Nusselt numbers based on the present model are found to be in better agreement with experimental data; the similarity solution (based on the boundary approximation, Darcy law with no thermal dispersion in an infinite constant porosity medium) is found to be accurate for the media Rayleigh number greater than 30.

1. INTRODUCTION

A GREAT deal of attention has been given to the study of natural convection in enclosures filled with a fluid-saturated porous medium during the past decades. Numerous theoretical studies have been performed for natural convection in enclosed rectangular porous cavities with two opposing walls being kept at different temperatures and the other walls being insulated [1, 2]. Most of the early studies were based on Darcy's law with the assumption of a constant porosity medium. Results of these investigations show that the Nusselt number depends on the Rayleigh number and the aspect ratio. However, experimental results [3, 4] show that the Nusselt number depends not only on the parameters mentioned above, but also on the Prandtl number, the Darcy number and the thermal conductivity ratio of the fluid to solid phases. The discrepancy between theory and experiments has prompted researchers to use new models for the prediction of fluid flow and heat transfer characteristics in porous media. For example, Prasad and Tuntomo [5] used the Darcy–Forchheimer equation to study the inertia effect on natural convection in a vertical porous cavity. Tong and Subramanian [6] used the Darcy–Brinkman model to study the boundary effect on natural convection in porous enclosures. Davis *et al.* [7] used the Darcy–Brinkman–Forchheimer model to study the same problem with variable porosity effects taken into consideration. Hsiao *et al.* [8] used the macroscopic momentum equation obtained by Hsu and Cheng [9] to study natural convection about a horizontal cylinder in a porous enclosure with effects of non-uniform porosity and permeability, no-slip boundary conditions, micro- and macro-inertia and thermal dispersion taken into consideration.

Recently, the problem of natural convection in a porous cavity with discrete heat sources has attracted considerable attention. For example, El-Knatib and Prasad [10] and Robillard *et al.* [11] studied the problems of steady natural convection in porous cavities with a localized heat source from below. The formulation of the problem was based on the Darcy law and a constant porosity medium. In this paper, we shall study the effects of non-Darcy, variable porosity

NOMENCLATURE

A	aspect ratio of the cavity, L_2/L_1
a, b	Ergun constants
B	constant defined in equation (11)
C	thermal dispersivity
C_p	specific heat at constant pressure
Da	Darcy number, K/H_2^2
Da_∞	bulk Darcy number
E	distance between the centerline of the heated plate and the centerline of the wall
e	eccentricity of the heat source, $E/(H_2/2)$
F	Forchheimer coefficient
f	quantity defined in equation (25)
g	gravitational acceleration
H_1	distance between the top of the heated plate and the top of the wall
H_2	length of the plate
H_3	distance between the bottom of the plate and the bottom of the wall
h	heat transfer coefficient
K	permeability
K_∞	bulk permeability
k_c	stagnant thermal conductivity
$k_{c\infty}$	bulk stagnant thermal conductivity
k_d	dispersive thermal conductivity
k_e	effective thermal conductivity of the porous medium
k_f	thermal conductivity of the fluid phase
k_s	thermal conductivity of the solid phase
L_1	width of the cavity
L_2	height of the cavity
m	number of iteration
Nu	local Nusselt number based on the thermal conductivity of the fluid
$\overline{Nu}$	mean Nusselt number based on the thermal conductivity of the fluid
Nu_m	local media Nusselt number
$\overline{Nu}_m$	mean media Nusselt number
Pr_f	Prandtl number of the fluid phase
p^*, p	dimensional and dimensionless pressures
Ra	Rayleigh number of fluid, $g\beta_f(T_h^* - T_c^*)H_2^3/\upsilon_f\alpha_f$
Ra_m	media Rayleigh number
T^*, T	dimensional and dimensionless temperatures
u^*, u	dimensional and dimensionless Darcian velocities in the x^*-direction
v^*, v	dimensional and dimensionless Darcian velocities in the y^*-direction
x^*, x	dimensional and dimensionless horizontal coordinates
Y	dimensionless y coordinate based on height of the cavity
y^*, y	dimensional and dimensionless vertical coordinates.

Greek symbols

α_e	effective thermal diffusivity, $k_e/\rho_f C_{pf}$
α_f	thermal diffusivity of fluid, $k_f/\rho_f C_{pf}$
β_f	thermal expansion coefficient of fluid
Γ	dimensionless particle diameter, d_p/H_2
θ	inclination angle of the cavity
λ	thermal conductivity ratio of fluid and solid phases
μ_f	dynamic viscosity of fluid
ν_f	kinematic viscosity of fluid
ρ_f	density of fluid
ϕ	porosity
Ψ	dimensionless stream function
Ω	dimensionless vorticity
∇^2	Laplace operator in the (x, y) coordinates.

and thermal dispersion on natural convection in an inclined porous cavity with a discrete heat source on one wall. The mathematical formulation of the problem follows the previous work by Hsiao *et al.* [8]. A numerical solution was obtained based on the finite difference method. It is found that a secondary vortex begins to appear downstream of the discrete heat source when convection begins to predominate. The intensity of this vortex increases with the eccentricity of the heat source and the inclined angle of the cavity.

2. MATHEMATICAL FORMULATION

Consider an inclined two-dimensional rectangular porous cavity with height L_2 and width L_1, as shown in Fig. 1, where the x and y coordinates are fixed with the cavity. A heated plate with length H_2 kept at a temperature T_h^* is mounted on one wall, while the rest of the walls are kept at room temperature, T_c^*. The bottom of the cavity is tilted at an angle θ with respect to the horizon. The distance between the top of the cavity and the heated plate is H_1, while that between the bottom of the cavity and the heated plate is H_3. The distance between the centerline of the heated plate and the centerline of the wall is E, such that when $E = 0$ the heated plate is centrally located on the side wall. The eccentricity of the plate is defined as $e = E/(H_2/2)$. Thus, e is positive if the centerline of the heated plate is below the centerline of the wall, while e is negative if the centerline of the heated plate is above the centerline of the wall.

We now introduce the following dimensionless variables:

$$x = \frac{x^*}{H_2}, \quad y = \frac{y^*}{H_2}, \quad u = \frac{u^* H_2}{\alpha_f}, \quad v = \frac{v^* H_2}{\alpha_f},$$

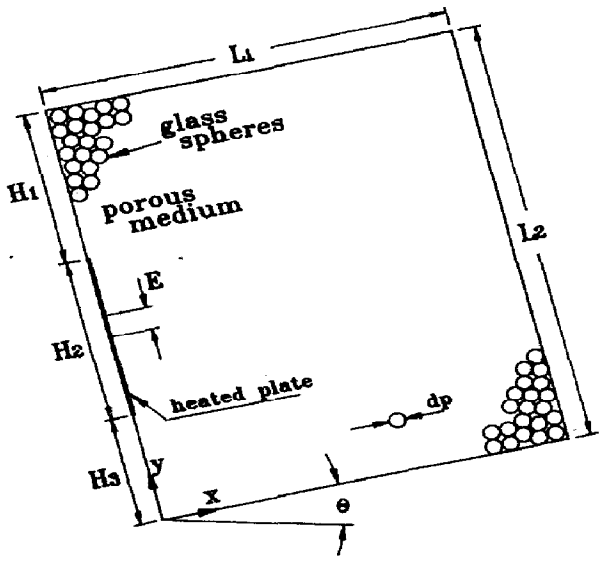

FIG. 1. Physical model and coordinate system.

$$T = \frac{T^* - T_c^*}{T_h^* - T_c^*}, \quad p = \frac{p^* H_2}{\rho_f \alpha_f^2}, \tag{1}$$

where x and y are the dimensionless horizontal and vertical coordinates; u^* and u are the dimensional and dimensionless Darcian velocities in the x-direction, while v^* and v are the dimensional and dimensionless Darcian velocities in the y-direction; p^* and p are the dimensional and dimensionless pressures; T^* and T are the dimensional and dimensionless temperatures; ρ_f and α_f are the density and thermal diffusivity of the fluid phase. The continuity equation in terms of these dimensionless variables is

$$\frac{\partial u}{\partial x} + \frac{\partial v}{\partial y} = 0. \tag{2}$$

The macroscopic dimensionless momentum equations for a variable porosity medium derived by Hsu and Cheng [9] are

$$u\frac{\partial}{\partial x}\left(\frac{u}{\phi}\right) + v\frac{\partial}{\partial y}\left(\frac{u}{\phi}\right) = -\frac{\partial p}{\partial x} + Pr_f \nabla^2 u - \left(\frac{Pr_f}{Da} + \frac{F}{\sqrt{Da}}|\bar{w}|\right)\phi u + Ra\, Pr_f\, \phi T \sin\theta \tag{3}$$

$$u\frac{\partial}{\partial x}\left(\frac{v}{\phi}\right) + v\frac{\partial}{\partial y}\left(\frac{v}{\phi}\right) = -\frac{\partial p}{\partial y} + Pr_f \nabla^2 v - \left(\frac{Pr_f}{Da} + \frac{F}{\sqrt{Da}}|\bar{w}|\right)\phi v + Ra\, Pr_f\, \phi T \cos\theta, \tag{4}$$

where ϕ is the porosity which is assumed to vary exponentially with distance from the walls, i.e.

$$\phi = \phi_\infty + (\phi_0 - \phi_\infty)\exp(-N_1 x/\Gamma) \tag{5}$$

with $\Gamma = d_p/H_2$ being the dimensionless particle diameter, N_1 being an empirical constant, while ϕ_0 and ϕ_∞ are the porosity on the wall and far away from the wall. In equations (3) and (4), F is the inertia coefficient, which is given by

$$F = \frac{b}{\sqrt{a}\,\phi^{3/2}}, \tag{6}$$

where a and b are Ergun's constants. The parameters Pr_f and Ra in equations (3) and (4) are the Prandtl number and the Rayleigh number of the fluid, which are defined as $Pr_f = \nu_f/\alpha_f$ and $Ra = g\beta_f(T_h^* - T_c^*)H_2^3/\alpha_f\nu_f$, where g is the gravitational acceleration, β_f and ν_f are the thermal expansion coefficient and the kinematic viscosity of the fluid. The parameter Da in equations (3) and (4) is the local Darcy number, defined as $Da = K/H_2^2$, where K is the local permeability of the medium, which is given by

$$K = \frac{\phi^3 d_p^2}{a(1-\phi)^2} \tag{7}$$

for a packed-sphere bed. The local Darcy number is related to the bulk Darcy number (Da_∞) by

$$Da = Da_\infty \frac{K}{K_\infty} = Da_\infty \left(\frac{\phi}{\phi_\infty}\right)^3 \left(\frac{1-\phi_\infty}{1-\phi}\right)^2, \tag{8}$$

where

$$Da_\infty = K_\infty/H_2^2 = \frac{\Gamma^2\phi_\infty^3}{a(1-\phi_\infty)^2},$$

with K_∞ denoting the bulk permeability.

The dimensionless energy equation is

$$u\frac{\partial T}{\partial x} + v\frac{\partial T}{\partial y} = \frac{\partial}{\partial x}\left(\frac{\alpha_e}{\alpha_f}\frac{\partial T}{\partial x}\right) + \frac{\partial}{\partial y}\left(\frac{\alpha_e}{\alpha_f}\frac{\partial T}{\partial y}\right). \tag{9}$$

In the above equation, α_e is the effective thermal diffusivity of the saturated porous medium, which is given by $\alpha_e = k_e/(\rho c_p)_f$, where k_e is the effective thermal conductivity of the porous medium, which is the sum of the stagnant thermal conductivity of porous medium k_c and the dispersive conductivity k_d, i.e.

$$k_e = k_c + k_d. \tag{10}$$

The stagnant thermal conductivity of the medium can be computed according to the following expression [12]:

$$\frac{k_c}{k_f} = (1-\sqrt{(1-\phi)}) + \frac{2\sqrt{(1-\phi)}}{1-\lambda B}\left[\frac{(1-\lambda)B}{(1-\lambda B)^2}\ln\left(\frac{1}{\lambda B}\right) - \frac{B+1}{2} - \frac{B-1}{1-\lambda B}\right], \tag{11}$$

where $B = 1.25[1-\phi/\phi]^{10/9}$ and $\lambda = k_f/k_s$, with k_f and k_s being the thermal conductivities of the fluid and the solid phases, respectively. The value of k_s for glass beads can be calculated according to [8]

$$k_s = 1.00416 + 1.6736\times10^{-3}T^* - 4.184\times10^{-6}T^{*2}, \tag{12}$$

where T^* is the temperature in °C and k_s is expressed

in W m^{-1} °C^{-1}. The thermal dispersion conductivity for flow through a porous medium is given by [9]

$$k_d = 0.02\left(\frac{1-\phi}{\phi}\right)(\rho C_p)_f |\bar{w}^*| d_p, \tag{13}$$

where $|\bar{w}^*| = (u^{*2}+v^{*2})^{1/2}$ and the constant 0.02 was obtained by matching theory with experiments [9].

We now introduce the dimensionless stream function Ψ and dimensionless vorticity Ω as

$$u = \frac{\partial \Psi}{\partial y}, \quad v = -\frac{\partial \Psi}{\partial x}, \tag{14}$$

$$\Omega = \frac{\partial v}{\partial x} - \frac{\partial u}{\partial y}. \tag{15}$$

Eliminating the pressure terms in equations (3) and (4) and expressing the resulting equations in terms of the dimensionless stream function Ψ and dimensionless vorticity Ω yield

$$\nabla^2 \Psi = -\Omega \tag{16}$$

$$\begin{aligned}
&\frac{\partial}{\partial x}\left[\frac{\partial \Psi}{\partial y}\frac{\partial}{\partial x}\left(-\frac{1}{\phi}\frac{\partial \Psi}{\partial x}\right) - \frac{\partial \Psi}{\partial x}\frac{\partial}{\partial y}\left(-\frac{1}{\phi}\frac{\partial \Psi}{\partial x}\right)\right] \\
&- \frac{\partial}{\partial y}\left[\frac{\partial \Psi}{\partial y}\frac{\partial}{\partial x}\left(\frac{1}{\phi}\frac{\partial \Psi}{\partial y}\right) - \frac{\partial \Psi}{\partial x}\frac{\partial}{\partial y}\left(\frac{1}{\phi}\frac{\partial \Psi}{\partial y}\right)\right] \\
&= Pr_f \nabla^2 \Omega - \left[\left(\frac{Pr_f}{Da} + \frac{F}{\sqrt{Da}}|\bar{w}|\right)\phi\right]\Omega + \frac{\partial \Psi}{\partial y}\frac{\partial}{\partial y} \\
&\times \left[\left(\frac{Pr_f}{Da} + \frac{F}{\sqrt{Da}}|\bar{w}|\right)\phi\right] + \frac{\partial \Psi}{\partial x}\frac{\partial}{\partial x} \\
&\times \left[\left(\frac{Pr_f}{Da} + \frac{F}{\sqrt{Da}}|\bar{w}|\right)\phi\right] \\
&+ Ra\, Pr_f\left[\frac{\partial}{\partial x}(\phi T)\cos\theta - \frac{\partial}{\partial y}(\phi T)\sin\theta\right].
\end{aligned} \tag{17}$$

The energy equation in terms of the dimensionless stream function Ψ is

$$\frac{\partial \Psi}{\partial y}\frac{\partial T}{\partial x} - \frac{\partial \Psi}{\partial x}\frac{\partial T}{\partial y} = \frac{\partial}{\partial x}\left(\frac{\alpha_e}{\alpha_f}\frac{\partial T}{\partial x}\right) + \frac{\partial}{\partial y}\left(\frac{\alpha_e}{\alpha_f}\frac{\partial T}{\partial y}\right). \tag{18}$$

The dimensionless boundary conditions are

$$\frac{\partial \Psi}{\partial x} = \Psi = 0, \quad T = 1, \quad \Omega = -\Psi_{xx},$$

$$\text{at } x = 0, \quad \frac{H_3}{H_2} \leqslant y \leqslant \frac{H_2+H_3}{H_2} \tag{19}$$

$$\frac{\partial \Psi}{\partial x} = \Psi = T = 0, \quad \Omega = -\Psi_{xx},$$

$$\text{at } x = 0, \quad 0 \leqslant y \leqslant \frac{H_3}{H_2} \tag{20}$$

$$\frac{\partial \Psi}{\partial x} = \Psi = T = 0, \quad \Omega = -\Psi_{xx},$$

$$\text{at } x = 0, \quad \frac{H_2+H_3}{H_2} \leqslant y \leqslant \frac{L_2}{H_2} \tag{21}$$

$$\frac{\partial \Psi}{\partial x} = \Psi = T = 0, \quad \Omega = -\Psi_{xx},$$

$$\text{at } x = \frac{L_1}{H_2}, \quad 0 \leqslant y \leqslant \frac{L_2}{H_2} \tag{22}$$

$$\frac{\partial \Psi}{\partial y} = \Psi = T = 0, \quad \Omega = -\Psi_{yy},$$

$$\text{at } 0 \leqslant x \leqslant \frac{L_1}{H_2}, \quad y = 0 \tag{23}$$

$$\frac{\partial \Psi}{\partial y} = \Psi = T = 0, \quad \Omega = -\Psi_{yy},$$

$$\text{at } 0 \leqslant x \leqslant \frac{L_1}{H_2}, \quad y = \frac{L_2}{H_2}. \tag{24}$$

3. NUMERICAL PROCEDURES

The governing equations (16)–(18) subject to boundary conditions (19)–(24) with auxiliary equations (5)–(8) and (10)–(13) were discretized by the finite difference method based on second-order differencing, and the resulting finite difference equations were solved by the successful over-relaxation (SOR) technique. The iterative process was terminated until the following convergence criterion was satisfied:

$$\left|\frac{f^{m+1} - f^m}{f^{m+1}}\right| \leqslant 10^{-4}, \tag{25}$$

where f stands for Ψ, Ω and T, while m is the iteration number.

After the convergence criterion had been satisfied, computations were carried out for the local and mean Nusselt numbers along the discrete heat source, which are defined as

$$Nu = \frac{hH_2}{k_f} = -\left.\frac{\partial T}{\partial x}\right|_{x=0} \tag{26a}$$

$$\overline{Nu} = \frac{1}{H_2}\int_{H_3}^{H_3+H_2} Nu(y)\,dy. \tag{26b}$$

The values of Nu and $\overline{Nu}$ are related to the local media Nusselt number Nu_m and the mean media Nusselt number $\overline{Nu}_m$ by

$$Nu = \frac{k_{c\infty}}{k_f} Nu_m \tag{27a}$$

$$\overline{Nu} = \frac{k_{c\infty}}{k_f}\overline{Nu}_m. \tag{27b}$$

Similarly, the Rayleigh number Ra is related to the media Rayleigh number Ra_m by

$$Ra = Ra_m\, Da\,(\alpha_{c\infty}/\alpha_f), \tag{28}$$

where

$$Ra_m = g\beta_f(T_h^* - T_c^*)H_2/\alpha_{c\infty}\nu_f.$$

Table 1. Comparisons of Nusselt numbers between the present and Robillard *et al.*'s numerical results [11] for a discrete heat source on the bottom surface of a porous cavity

Condition	H_2/L_2	e	Ra_m	A	Present results	Robillard *et al.* [11]
	0.28	0.36	50	1	1.79	1.77
Localized	0.28	0.36	100	1	2.92	2.89
heating	0.28	0.36	150	1	3.68	3.64
from	0.28	0.36	200	1	4.31	4.22
below	0.5	0	100	1	2.55	2.50
	0.5	0	150	1	3.72	3.68
($\theta = 90°$)	0.5	0	200	1	4.60	4.52

4. RESULTS AND DISCUSSION

The parameters shown in the governing equations and boundary conditions are the particle diameter, Rayleigh number, Prandtl number, Darcy number, the eccentricity of the heat source, aspect ratio of the cavity, the thermal conductivity ratio of fluid to solid phases, porosity and inclination angle of the cavity. Numerical solutions were first carried out for a square cavity having $H_1 = 7.5''$ (19.05 cm), $H_2 = 18''$ (45.72 cm), $H_3 = 3.5''$ (8.89 cm), $L_2 = 29''$ (73.66 cm), i.e. $e = 0.138$, which correspond to the experimental apparatus used by Cheng *et al.* [13]. To study the effect of eccentricity of the heat source, other values of e (while keeping the same values of H_2 and L_2) were also computed. Other constants used in the numerical calculations were $\phi_\infty = 0.36$, $\phi_0 = 0.9$, $N_1 = 7$, $a = 215$ and $b = 1.92$, and $Pr_f = 4.3$ and $\lambda = 0.6$ for a water/glass spheres system and $Pr_f = 160$ and $\lambda = 0.14$ for a silicone oil/glass spheres system. Since four differential theoretical models are considered, the following symbols are used: CPND denotes constant porosity without dispersion, CPWD denotes constant porosity with dispersion, VPND denotes variable porosity without dispersion and VPWD denotes variable porosity with dispersion. In all of these models, no-slip boundary conditions were imposed.

Accuracy of the numerical solution

As mentioned earlier, Robillard *et al.* [11] have carried out a numerical solution based on the Darcy law without dispersion for natural convection in a constant porosity cavity with a discrete heat source on the bottom surface. To assess the accuracy of the numerical algorithm used in this paper, computations were also carried out under the same conditions. It was found that a uniform grid of 81×81 was sufficient for $Pr_f < 5$ and moderate media Rayleigh numbers ($Ra_m < 150$). However, for higher values of the media Rayleigh number and Prandtl number, a uniform grid of 101×101 is needed for the same accuracy. Table 1 is a comparison of Robillard *et al.*'s numerical results and those based on the present numerical algorithm. It is shown that results based on the present algorithm agree very well with those obtained by Robillard *et al.* [11].

Comparison with experimental results

Inaba *et al.* [4] have performed an experiment on natural convection in an inclined porous cavity heated at constant temperatures at opposing walls and thermally insulated at other walls. Table 2 is a comparison of the average media Nusselt numbers obtained experimentally by Inaba *et al.* [4] and the present numerical solutions based on four theoretical models for natural convection in rectangular cavities filled with glass spheres saturated with water at zero inclination angle ($\theta = 0°$) with $A = 5$ and $\Gamma = 0.153$. It is shown that the numerical results with variable porosity and thermal dispersion effects taken into consideration agree the best with experimental data.

Onset of free convection

Figure 2 shows the effect of the fluid Rayleigh number on $\overline{Nu}/\overline{Nu}_c$ (where $\overline{Nu}_c$ is the Nusselt number for heat conduction) with $\Gamma = 0.1$, $e = 0.138$ and $\lambda = 0.6$ for a cavity at zero inclination angle ($\theta = 0$) based on four different models. As indicated in the figure, the Nusselt number is the highest for the model with variable porosity and thermal dispersion (VPWD) taken into consideration, while the Nusselt number is smallest for the constant porosity model with no thermal dispersion (CPND) taken into consideration. Note that the curves begin to deviate from the horizontal line at unity between $Ra = 5 \times 10^5$ and 7×10^5 (corresponding to $Ra_m = 2.6$–3.7), depending on the particular model used. These are the critical Rayleigh numbers for the onset of free convection in a porous cavity at zero inclination angle. From this figure, it can be concluded that the variable porosity and thermal dispersion effects enhance instability.

Streamlines and isotherms

Figure 3 shows the isotherms (left) and streamlines (right) in a constant porosity cavity with $A = 1$ at $Ra_m = 53$ (corresponding to $Ra = 10^7$ and $\Gamma = 0.1$), $\lambda = 0.6$, $e = 0.138$, and $\theta = 0$, 45° and 90°. For the case of zero inclination angle and $Ra_m = 53$, it is shown that a small secondary vortex begins to appear downstream of the heated plate in the upper corner of the porous cavity. The strength of the secondary vortex increases with inclination angle. To investigate

Table 2. Comparisons of Nusselt numbers between present and previously published experimental results

Porous media	Γ	A	Ra_m	θ	Inaba *et al.* [4]	Present results			
						VPWD	VPND	CPWD	CPND
Water/glass	0.153	5	121	0	3.64	3.124	3.014	2.441	2.287
Water/glass	0.153	5	1260	0	9.71	9.132	8.724	7.643	7.321

the reason for the appearance of the secondary vortex, computations were carried out with the same parameters as those in Fig. 3, except the discrete heat source was replaced by a wall at a uniform temperature. The results for streamlines (not presented) show that there is no secondary vortex. It can be concluded, therefore, that the appearance of the secondary vortex is due to the existence of the discrete heat source. To examine the effect of eccentricity of the discrete heat source on the heat transfer and the flow pattern, numerical solutions were carried out for $Ra_m = 53$ (corresponding to $Ra = 10^7$ and $\Gamma = 0.1$), $\lambda = 0.6$, and $\theta = 30°$ at $e = 0$, 0.138 and 0.379. The results of these computations are presented in Fig. 4. It is shown that the lower the location of the discrete heat source (i.e. larger value of e), the stronger the strength of the secondary vortex and hence the higher the heat flux.

Temperature distribution

The effect of eccentricity of the discrete heat source on temperature distribution along the vertical axis of a square cavity filled with glass spheres saturated with silicone oil ($Pr_f = 160$) is presented in Fig. 5(a), while those saturated with water ($Pr_f = 4.3$) are presented in Fig. 5(b). The results are based on the CPWD model with the discrete heat source located on the bottom surface of the cavity. It is shown that the temperature inversion is more pronounced at a larger eccentricity, suggesting the convection effect is stronger when the discrete heat source is located closer to the bottom of the cavity. A comparison of Figs. 5(a) and (b) indicates that temperature inversion in the silicone oil/glass spheres system ($Pr_f = 160$) is not as severe as in the water/glass spheres system ($Pr_f = 4.3$) due to the higher viscosity of the silicone oil and therefore a smaller convection velocity.

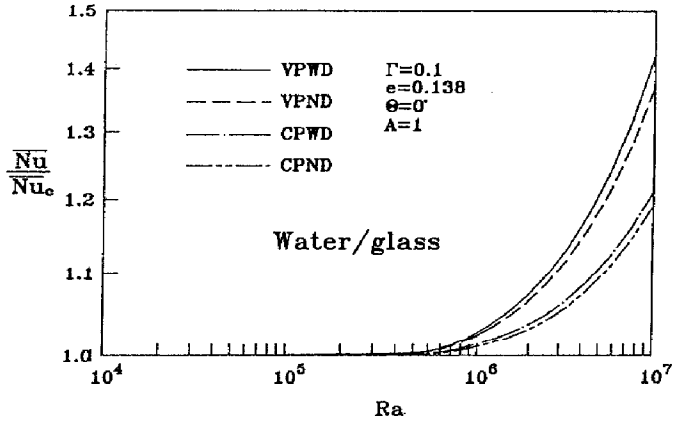

FIG. 2. Normalized mean Nusselt number for a square cavity at zero inclination angle with $\Gamma = 0.1$, $e = 0.138$ and $\lambda = 0.6$ calculated from four different models.

Heat transfer

Figure 6 shows the effect of inclination angle on heat transfer in a constant porosity cavity with isothermal opposing walls at different temperatures and with other walls being thermally insulated at a high media Rayleigh number of 530 (corresponding to $Ra = 10^8$ and $\Gamma = 0.1$) for which the free convection current is strong. It is shown that a maximum value of the Nusselt number exists at $\theta = 30°$, and that the Nusselt number at $\theta = 0°$ (i.e. vertical heated wall) is higher than that at $\theta = 90°$ (i.e. horizontally heated wall). This behavior is in qualitative agreement with Inaba *et al.*'s data.

Figure 7 shows the effects of thermal dispersion and

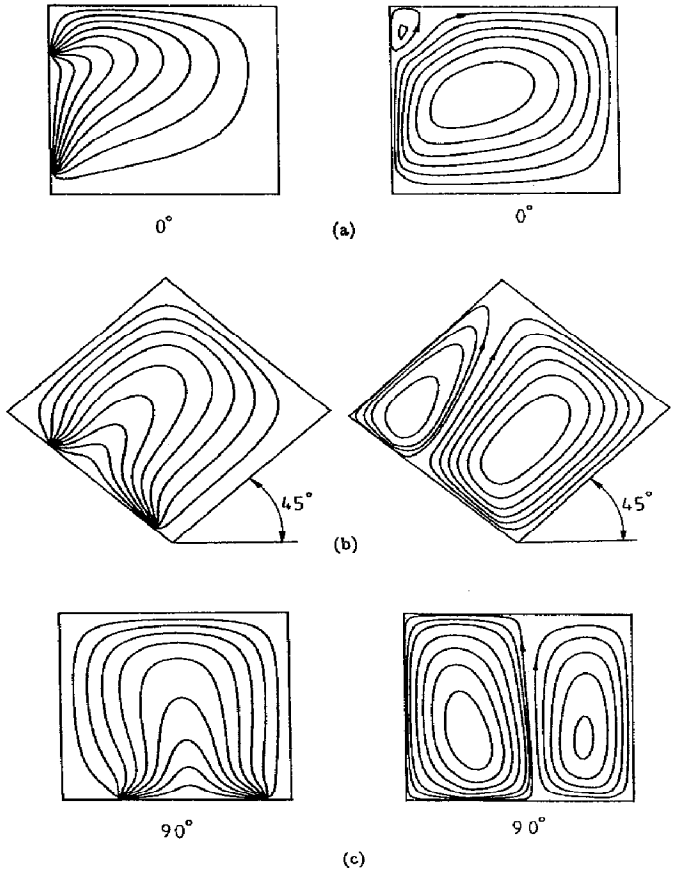

FIG. 3. Effects of inclination of the discrete heat source on isotherms (left, $\Delta T = 0.1$) and streamlines (right, $\Delta\Psi = 1$) for $Ra = 10^7$, $\Gamma = 0.1$ and $\lambda = 0.6$.

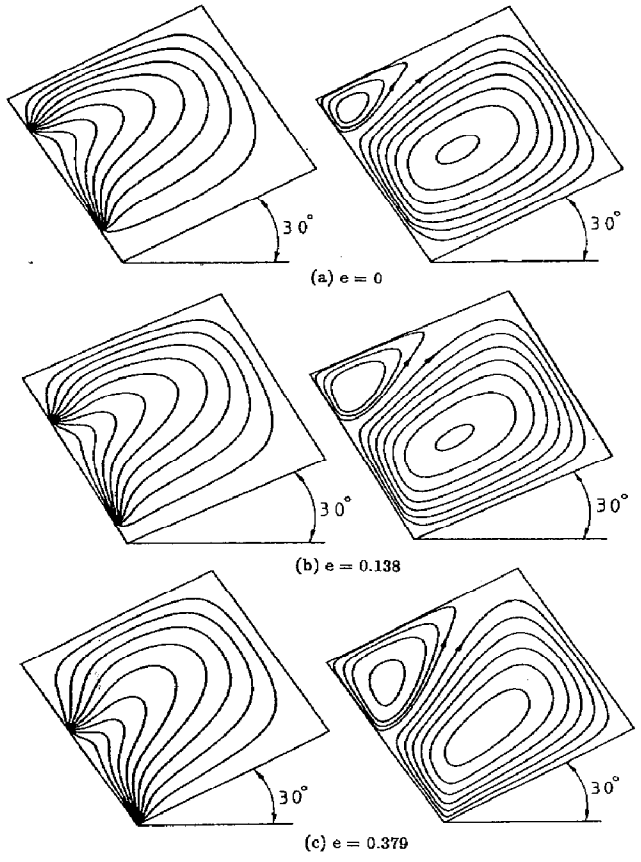

FIG. 4. Effects of eccentricity of the discrete heat source on isotherms (left, $\Delta T = 0.1$) and streamlines (right, $\Delta\Psi = 1$) for $Ra = 10^7$, $\Gamma = 0.1$, $e = 0.138$, $\lambda = 0.6$ and $\theta = 30°$.

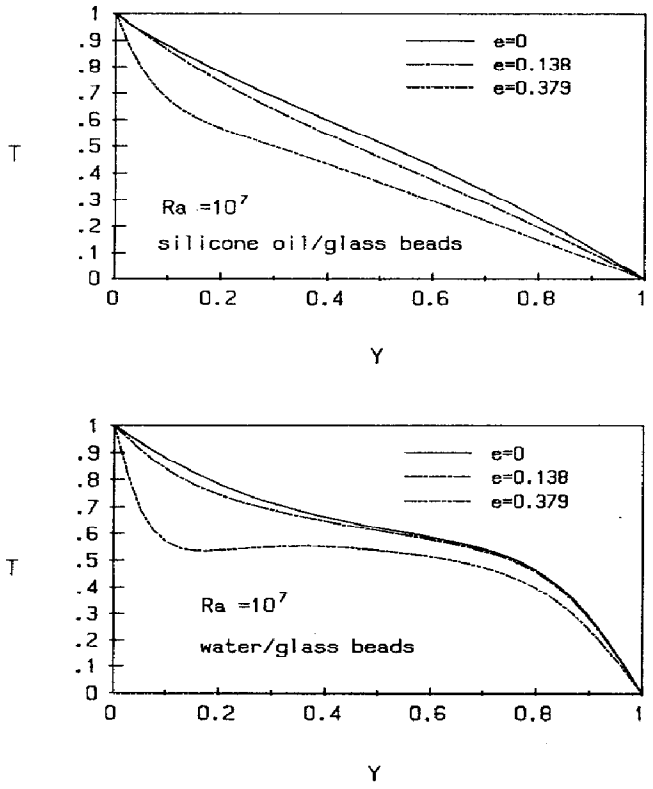

FIG. 5. Effects of eccentricity of the heat source on the temperature distribution along the vertical axis of a square constant porosity cavity heated from below. (a) Silicone oil/glass ($Pr_f = 160$). (b) Water/glass ($Pr_f = 4.3$).

inclination angle on the mean fluid Nusselt number for a water/glass spheres system with $e = 0.138$ at low to moderate media Rayleigh numbers from 5.3 (corresponding to $Ra = 10^6$ and $\Gamma = 0.1$) to 53 (corresponding to $Ra = 10^7$ and $\Gamma = 0.1$), assuming a constant porosity medium. It can be concluded that (1) thermal dispersion tends to increase the heat transfer rate, (2) the effect of thermal dispersion is more pronounced at a higher Rayleigh number, (3) the effect of thermal dispersion on heat transfer is not influenced by the inclination angle of the cavity for $Ra_m < 5.3$, where conduction is predominant, and (4) at a moderate Rayleigh number ($Ra_m = 53$, for example), the mean Nusselt number increases to a maximum and then decreases; the effect of thermal dispersion increases with the inclination angle of the cavity.

Figure 8 shows the effects of dimensionless particle diameter and inclination angle on the mean Nusselt number based on the VPWD model for $e = 0.138$, $\lambda = 0.6$ and $Ra = 10^7$. It can be concluded from this graph that the heat transfer rate is not influenced by the dimensionless particle diameter and the inclination angle for $\Gamma < 0.01$. This corresponds to $Ra_m = 0.53$, which is below the critical media Rayleigh number for the onset of convection, i.e. heat is transferred by conduction. With further increase in the dimensionless particle diameter to 0.1 (corresponding to $Ra_m = 53$), the heat transfer rate first decreases with the inclination angle from 0° to 45° and then increases with inclination angle from 45° to 90°, which means a minimum heat transfer rate occurs at the inclination angle about 45°. Comparing Figs. 6 and 7, it is noted that the behavior of the Nusselt number at moderate Rayleigh number ($Ra_m = 53$) as a function of the inclination angle depends greatly on whether the porosity is assumed to be constant or variable.

Figure 9 shows the effects of variable porosity and the eccentricity of the discrete heat source on the mean fluid Nusselt number for a water/glass spheres system

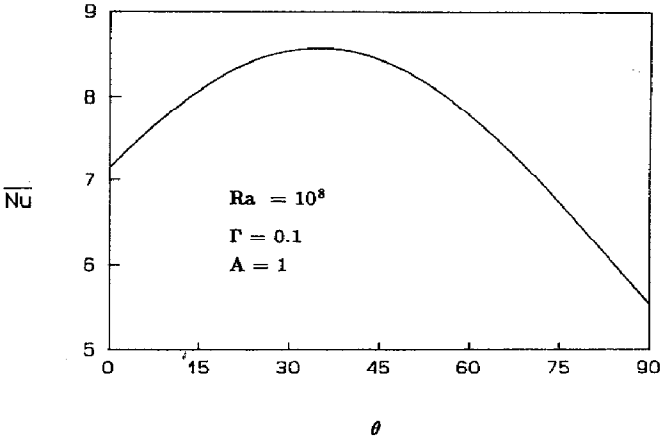

FIG. 6. Effects of inclination angle on the mean Nusselt number in a constant porosity cavity at a high media Rayleigh number ($Ra_m = 530$).

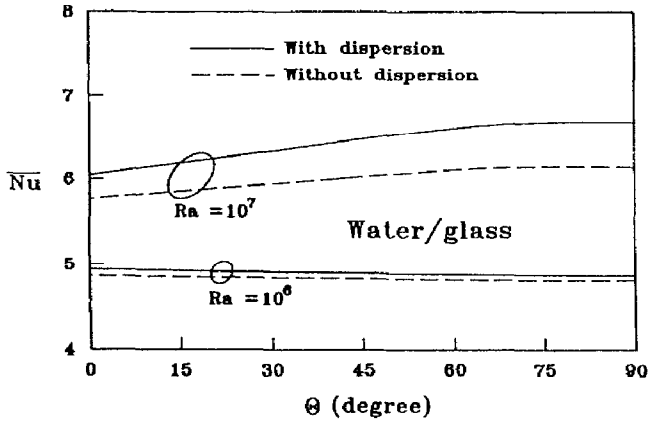

FIG. 7. Effects of thermal dispersion and inclination angle on the mean Nusselt number in a uniform porosity cavity at low to moderate media Rayleigh numbers ($Ra_m = 5.3$–53) and $e = 0.138$.

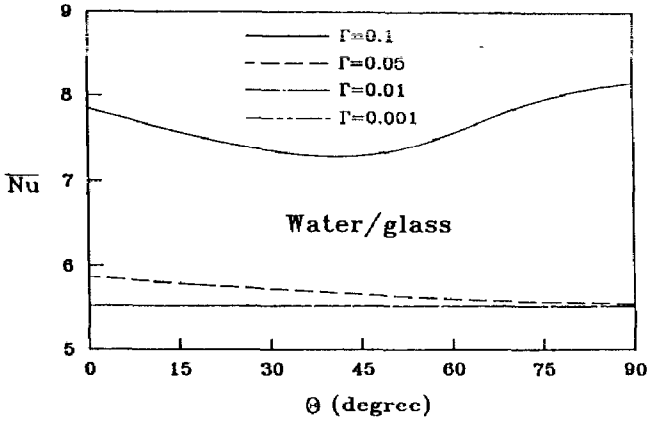

FIG. 8. Effect of particle diameter and inclination angle on the mean Nusselt number in a variable porosity cavity at low media Rayleigh numbers ($Ra_m = 0.053$–53) with $\lambda = 0.6$ and $e = 0.138$.

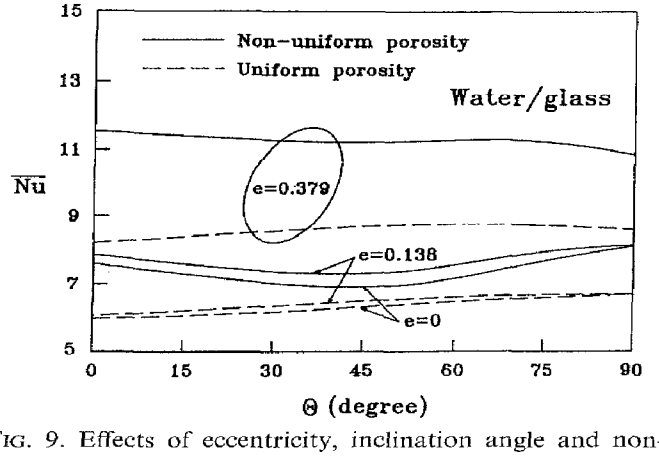

FIG. 9. Effects of eccentricity, inclination angle and non-uniform porosity on the mean Nusselt number at a moderate media Rayleigh number ($Ra_m = 53$) with $\lambda = 0.6$.

at various inclination angles at a moderate media Rayleigh number of 53 (corresponding to $Ra = 10^7$ and $\Gamma = 0.1$) and $\lambda = 0.6$. It can be seen that the effect of variable porosity tends to increase the heat transfer rate, and that the heat transfer rate increases with

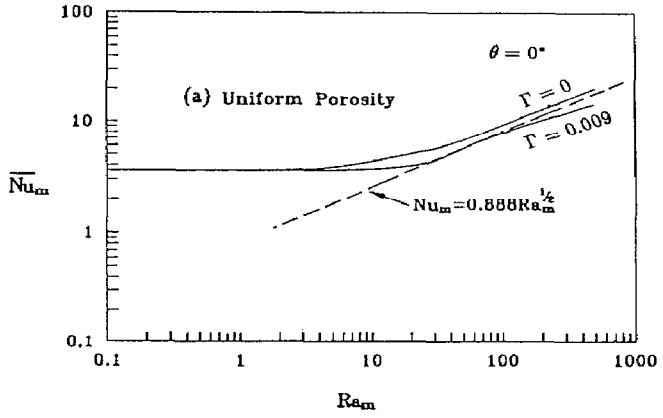

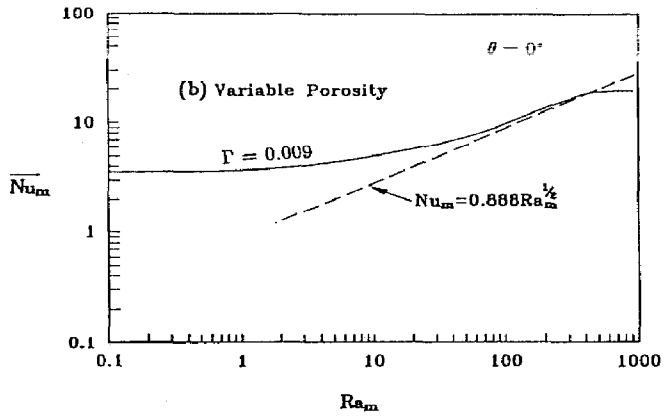

FIG. 10. Comparison of the similarity solution with present numerical solution on the mean media Nusselt number for natural convection about a vertical plate in a uniform porosity cavity (a) and a variable porosity cavity (b).

larger eccentricity. The behavior of the mean Nusselt number as a function of inclination at a moderate media Rayleigh number depends on whether the medium is assumed to be of constant or variable porosity, the eccentricity of the heat source and the Prandtl number of the fluid.

Comparison with the similarity solution

Figure 10(a) is a log–log plot of the mean media Nusselt number versus media Rayleigh number for natural convection in a constant porous cavity at zero inclination angle. The straight dashed line is Cheng and Minkowycz's similarity solution [14] for natural convection about a semi-infinite vertical heated plate embedded in a constant porosity medium of infinite extent, which is given by

$$\overline{Nu}_m = 0.888 Ra_m^{1/2}. \quad (29)$$

The above equation is based on Darcy's law with boundary layer approximation and without thermal dispersion in a constant porosity medium. The solid line with $\Gamma = 0$ is the numerical solution based on Darcy's law without the boundary layer approxi-

mation and thermal dispersion in a constant porosity medium. Since the solid line approaches the straight line given by equation (29) asymptotically, it indicates that the boundary layer approximation is valid for $Ra_m > 30$. The solid curve with $\Gamma = 0.009$ represents results with the effects of shearing stress, the inertia and thermal dispersion taken into consideration. The fact that this solid curve is below the similarity solution at high media Rayleigh numbers suggests that the Brinkman and the inertia effects predominate over the thermal dispersion effect at these media Rayleigh numbers in a constant porosity medium. The corresponding results based on a variable porosity model, with thermal dispersion taken into consideration, are presented as a solid curve in Fig. 10(b), which lies above the similarity solution for $Ra_m < 200$. This suggests that the variable porosity and thermal dispersion effects are predominant at low media Rayleigh numbers. However, the solid curve crosses over the straight line at $Ra_m > 200$, indicating that the shearing stress and inertia effects are predominant over the thermal dispersion and variable porosity effects at high media Rayleigh numbers. The numerical results are in qualitative agreement with Cheng *et al.*'s data [13].

5. CONCLUDING REMARKS

Various effects on steady natural convection in an inclined porous cavity with a discrete heat source on a wall have been investigated in this paper. The following conclusions can be drawn.

1. At a sufficiently high media Rayleigh number, a secondary vortex begins to appear downstream of the discrete heat source. The strength of this vortex increases with the inclination angle of the porous cavity.
2. For a constant porosity medium, the effect of thermal dispersion is unimportant in comparison with the effects of inertia and shearing stress.
3. If the vertical wall of a constant porosity cavity is maintained at a constant temperature, Cheng and Minkowycz's similarity solution can be applied for the calculation of the heat transfer rate if the media Rayleigh number is higher than 30.
4. The variable porosity effect is predominant over the inertia and the shearing stress effects at low media Rayleigh numbers. However, the inertia and shearing stress effects are predominant over the variable porosity and thermal dispersion effects at high media Rayleigh numbers.
5. The eccentricity of the discrete heat source has an important effect on the heat transfer rate. The closer the heat source to the bottom wall, the higher the heat transfer rate.
6. The effect of inclination angle of the cavity on heat transfer depends on whether conduction or free convection predominates. At low media Rayleigh numbers, where conduction is predominant, the inclination angle has little effect on heat transfer. At intermediate Rayleigh numbers, the effect of inclination angle on the Nusselt number depends on the eccentricity of the heat source, the Prandtl number of the fluid and on whether the porosity is assumed to be constant or variable. At high media Rayleigh numbers, where free convection is predominant, the heat transfer rate increases to a maximum and then decreases as the inclination angle increases; moreover, the heat transfer rate at zero inclination angle is higher than at an inclination angle of 90

REFERENCES

1. P. Cheng, Heat transfer in geothermal systems, *Adv. Heat Transfer* **105**, 1–101 (1978).
2. D. A. Nield and A. Bejan, *Convection in Porous Media*. Springer, New York (1991).
3. N. Seki, S. Fukusako and H. Inaba, Heat transfer in a confined rectangular cavity packed with porous media, *Int. J. Heat Mass Transfer* **21**, 985–989 (1978).
4. H. Inaba, M. Sugawara and J. Blumenberg, Natural convection heat transfer in an inclined porous layer, *Int. J. Heat Mass Transfer* **31**, 1365–1374 (1988).
5. V. Prasad and A. Tuntomo, Inertia effects on natural convection in a vertical porous cavity, *Numer. Heat Transfer* **11**, 295–320 (1987).
6. T. W. Tong and E. Subramanian, A boundary layer analysis for natural convection in vertical porous enclosures, *Int. J. Heat Mass Transfer* **28**, 563–571 (1985).
7. E. Davis, G. Lauriat and P. Cheng, A numerical solution of variable porosity effects on natural convection in a packed-sphere cavity, *J. Heat Transfer* **113**, 391–399 (1991).
8. S. W. Hsiao, P. Cheng and C. K. Chen, Nonuniform porosity and thermal dispersion effects on natural convection about a heated horizontal cylinder in an enclosed porous medium, *Int. J. Heat Mass Transfer* **35**, 3407–3418 (1992).
9. C. T. Hsu and P. Cheng, Thermal dispersion in porous media, *Int. J. Heat Mass Transfer* **33**, 1587–1597 (1990).
10. G. El-Knatib and V. Prasad, Effects of stratification on thermal convection in horizontal porous layers with localized heating from below, *J. Heat Transfer* **109**, 683–687 (1987).
11. L. Robillard, C. H. Wang and V. Vasseur, Multiple steady states in a confined porous medium with localized heating from below, *Numer. Heat Transfer* **13**, 91–110 (1988).
12. P. Zehner and E. U. Schlunder, Thermal conductivity of granular materials at moderate temperatures (in German), *Chemie-Ingr.-Tech.* **42**, 933–941 (1970).
13. P. Cheng, C. L. Ali and A. K. Verma, An experimental study of non-Darcian effects in free convection in a saturated porous medium, *Lett. Heat Mass Transfer* **8**, 261–265 (1981).
14. P. Cheng and W. J. Minkowycz, Free convection about a vertical flat plate embedded in a porous medium with application to heat transfer from a dike, *J.G.R.* **82**, 2040–2044 (1977).